clean technologies

MDPI

Article

Modeling of CO_2 Capture by Electro-Swing Reactive Adsorption from Low-Concentration Streams

Célisse Chevrel [1,2], Paul de Joannis [1,3], Christophe Castel [3] and Olivier Authier [1,*]

[1] EDF R&D, 6 Quai Watier, 78400 Chatou, France
[2] MINES Paris, PSL–Research University, CEEP–Centre Energie, Environnement, Procédés, 60 Boulevard Saint-Michel, 75006 Paris, France
[3] Université de Lorraine, CNRS, LRGP, 54000 Nancy, France
* Correspondence: olivier.authier@edf.fr

Abstract: This article investigates the performance of Faradaic electro-swing reactive adsorption (ESA) for CO_2 capture using simulations. Traditional methods such as amine scrubbing face energy efficiency challenges, particularly at low CO_2 concentrations. ESA, which uses electricity for CO_2 regeneration, offers a promising alternative due to its isothermal operation and scalability. The study models ESA using quinone-based redox-active CO_2 carriers in an electrochemical cell with an ionic liquid electrolyte, allowing reversible adsorption and release through voltage control. The model estimates system productivity and energy consumption, considering transport and chemical kinetics. Key findings show that operating parameters, such as applied potential and gas flow rate, have a significant effect on efficiency. Applying a potential of −1.3 V improved the adsorption capacity, reducing CO_2 capture time compared to −1.1 V. At a 1% CO_2 concentration and a low flow rate, effective capture resulted in a productivity of 1.6 kg/(m^3·day) with an energy consumption of 0.6 MWh/tCO_2. However, higher gas flow rates reduced capture efficiency due to CO_2 transport limitations in the ionic liquid. Optimization of electrode design is essential to improve ESA efficiency.

Keywords: CO_2 capture; electrochemistry modeling; electro-swing; quinone

check for updates

Academic Editor: Shunde Yin

Received: 17 December 2024
Revised: 5 February 2025
Accepted: 17 February 2025
Published: 21 February 2025

Citation: Chevrel, C.; de Joannis, P.; Castel, C.; Authier, O. Modeling of CO_2 Capture by Electro-Swing Reactive Adsorption from Low-Concentration Streams. *Clean Technol.* **2025**, 7, 18. https://doi.org/10.3390/cleantechnol7010018

Copyright: © 2025 by the authors. Licensee MDPI, Basel, Switzerland. This article is an open access article distributed under the terms and conditions of the Creative Commons Attribution (CC BY) license (https://creativecommons.org/licenses/by/4.0/).

1. Introduction

CO_2 capture and storage are being considered as a decarbonization technique to reduce industrial CO_2 emissions and achieve levels compatible with a 1.5 °C global warming. Traditional techniques for separating CO_2 from flue gases and ambient air have relied primarily on the effects of temperature and pressure to vary the affinity of a substance (solvent or adsorbent material) for CO_2. These techniques have been used in industry for decades to release CO_2 in a concentrated stream, such as in amine-based scrubbing or adsorption on porous materials, and are still being studied to improve cost and performance [1]. However, these processes face challenges related to material stability (e.g., thermal and oxidative degradation) and energy efficiency (e.g., energy-intensive thermal integration into existing plants or limited performance with low-concentration CO_2 streams). In response to these challenges, electrochemical techniques are an attractive alternative to temperature- or pressure-controlled capture in a CO_2 concentration range, typically ranging from 0.04% (ambient air) to a few % (industrial flue gases such as in primary aluminum smelters at ~1% or in silicon production plants at ~3–4%) [2–5]. Aluminum and silicon are two examples of carbon-intensive materials for which demand has increased rapidly in recent years [6]. Electrochemical processes, including pH-mediated systems, electrochemically mediated

amine regeneration, and selective electro-active CO_2 carrier molecules, operate using electricity instead of thermal energy to regenerate captured CO_2. The use of low-carbon and dispatchable electricity helps to limit the overall emission factor of the capture processes. Initially developed for air filtration in the aerospace industry, electrochemical separation of CO_2 from gas mixtures is a rapidly growing area for reducing the energy requirements of CO_2 capture processes [4]. Electrochemical processes can operate under isothermal conditions at or near-ambient conditions, with limited heating and cooling requirements, and can be adapted to a variety of applications and scales through modular units.

In recent years, there have been significant advancements in the development of redox-active CO_2 carrier molecules, such as quinone-based strong nucleophiles incorporated as part of a solid electrode. These molecules can undergo reversible redox reactions at ambient temperature by binding CO_2 under reducing conditions, with a significantly enhanced affinity for CO_2, and releasing it in the oxidized form, with a low affinity for CO_2 [7–14]. The process typically involves applying and modulating voltage using an external power source to an electrochemical cell with one or more anode–cathode pairs for subsequent CO_2 capture and release when the applied cell voltage is reversed. The energy demand is mainly dependent on the voltage and the specific charge. Electrochemical cells with parallel channel structures of controllable shape and thickness offer advantages such as a low pressure drop, high mass transfer rate, and high surface area exposed to gas. This configuration also makes it easy to stack cells in a parallel passage contactor system. Changes in the length or width of the cell have a direct effect on the total capacity. The gas flow channel should be thin, typically a few hundred microns, but not so thin as to cause an excessive pressure drop. The potential of redox-active CO_2 carrier molecules to produce concentrated CO_2 from low-concentration streams has been demonstrated in laboratory-scale modules up to proof-of-concept, aiming to apply this technique in both point source and direct air capture applications [10,11,14–16].

The incorporation of quinones as a solid sorbent in carbon capture devices continues to present a persistent challenge. Voskian and Hatton have developed a new cell architecture using polymeric quinone-based electrodes to capture and release CO_2 through quinone reduction and oxidation, respectively [10]. Thus, cathode reduction leads to reduced quinone complexation with dissolved CO_2 in a conductive substrate, while cathode oxidation results in CO_2 release. Their method, called "electro-swing reactive adsorption" (ESA), involves a cathode made of a quinone polymerized into a solid, i.e., carbon fiber coated with carbon nanotubes (CNTs) and poly(1,4-anthraquinone) (p-AQ). This allows for reversible adsorption of CO_2 contained in a gas mixture onto the electrode surface, with an exposed area of a typical cell of a few cm^2 to a few hundred cm^2. The cell also includes a carbon fiber anode coated with CNTs and polyvinyl ferrocene (PVFc). Within the system, CO_2 diffuses from the gas mixture in the channel to the electrolyte and the quinone sites, immobilized on a conductive substrate and wetted with a nonvolatile ionic liquid electrolyte. After CO_2 solubility and lateral diffusion into the electrolyte, the quinone sites undergo a two-electron redox reaction and form a complex with dissolved CO_2. Therefore, two effects are activated in the cell: the associative effect of the ionic liquid used as an electrolyte (absorption mechanism) and the electronic effect due to the electron reservoir of the electrode containing the quinones (reduction mechanism). Using the ambient temperature ionic liquid 1-butyl-3-methylimidazolium bis(trifluorosulfonyl)imide ([Bmim]-[TF_2N]) as both solvent and electrolyte (of negligible volatility, high electrochemical stability, high quinone solubility, and reasonable transport properties), the system experimentally achieved the 90% Faradaic efficiency in a pure CO_2 environment. Cell operation in the range of -1.3 to -0.5 V (i.e., ΔE of 0.8 V) allowed efficient CO_2 capture and release. In an open-cell configuration with CO_2 concentrations ranging from 0.6% to 10% in pure nitrogen, the electrodes showed high

CO_2 capture efficiency, even at low concentrations (i.e., CO_2 capacity independent of the inlet steam concentration), with minimal performance degradation after extensive cycling. The electrical requirement for CO_2 removal was determined to be 0.25–0.57 MWh/tCO_2 (i.e., 0.9–2.0 GJ/tCO_2). This takes into account the Faradaic efficiency (defined as the moles of CO_2 captured per moles of electron transferred) and the applied potential difference. Another electrochemical cell with stackable bipolar cells using poly(vinylanthraquinone) (PVAQ) has been tested recently at the laboratory stage with feed CO_2 concentrations as low as 0.04% in pure nitrogen [11]. A complete cyclic operation, i.e., six cycles with 800 s duration including capture phase, release phase, and flush phase, was carried out in a cell with a single electrode pair to demonstrate the Faradaic efficiency around 92% (difference between the applied charge and discharge potentials of 1.5 V). The optimal electrochemical voltage window was 1.2 V (or slightly above) from the tests of the bipolar stack with multiple electrode pairs. During the steady-state operation of the cell, the specific energy consumption, calculated as the sum of the electrical and pneumatic work over a cycle, is approximately 0.7 MWh/tCO_2 (i.e., 2.6 GJ/tCO_2). A challenge to be addressed using quinones and the ionic liquid is the effect on the long-term stability of substances present in the gas mixture (oxygen, moisture, particles, pollutants, etc.). For example, oxygen (O_2) has a lower solubility in ionic liquids such as [Bmim]-[Tf_2N] compared to carbon dioxide (CO_2). However, O_2 molecules present in air or flue gas may be present in the electrolyte. Therefore, if the quinone is not properly tuned, parasitic side reactions with O_2 can occur, which can alter the charge capacity of the cell in realistic operating conditions. This challenge has been identified and can be minimized by carefully tuning the electron density of the quinone to make it more selective for CO_2, e.g., using benzodithiophene quinone [14]. Furthermore, if the gas to be treated contains charged or polarizable particles, these particles can be affected by the electric field and undergo electrophoresis, leading to surface fouling [17].

In addition to testing, comprehensive modelling CO_2 capture over a full cycle is an efficient tool for analyzing the contribution of all physicochemical parameters (liquid–vapor thermodynamic equilibrium between CO_2 and electrolyte, chemical kinetics, transport phenomena, etc.), for estimating performance (sorption capacity, cycle time, etc.) under varying operating conditions (gas flow rate, CO_2 concentration, pressure change, etc.) and for scaling-up from laboratory to industrial applications [18]. Voskian and Hatton simulated the capture phase in batch and flow using COMSOL software for a 2D planar geometry, with the breakthrough point reflecting the overall capacity of the electrodes, including the ability of the material to bind CO_2 and the rate at which CO_2 is adsorbed [10]. They characterized the effect of inlet CO_2 concentration (ranging from 10% to 50%) and electrochemical voltage (applied cell potential ranging from -1.3 to -1.7 V) on current densities and breakthrough profiles (i.e., outlet CO_2 concentration vs. bed volumes, defined as the volume within the cell through which the gas flow and contact occur) under flow conditions. The gas phase profiles are related to dispersed plug flow, while significant CO_2 diffusion limitation in the electrode is identified. The impact of CO_2 solubility in the electrolyte on process performance was also highlighted, both in terms of work capacity, i.e., the sum of CO_2 dissolved in the electrolyte and that complexed with the quinone, and transport dynamics, i.e., CO_2 fluxes.

There are still several needs concerning the modeling of a complete cycle by the ESA process, including both CO_2 capture and release, which depend on the cell dimensions that influence CO_2 capture performance. This study develops a dynamic numerical model to describe the ESA process at atmospheric pressure, including both CO_2 capture and release phases for a complete cycle, by representing an electrochemical cell using quinone-type CO_2 carrier molecules immobilized on the electrodes and an ionic liquid electrolyte. The model

represents the main phenomena coupling transport and chemical kinetics in the process to estimate the capture productivity and specific energy consumption of the system. It focuses on a configuration with parallel planes where CO_2 is present within the cell, such as the gas flow channel and the quinone electrode. The results of testing the sensitivity of global productivity and performance to the applied cell voltage and gas flow rate are presented.

2. Modeling

A schematic diagram of the cell geometry is shown in Figure 1. In the gas channel, gas flows from the inlet at y = 0 in the positive y direction and exits at the opposite side. The present dynamic model is based on the following equations at the scale of an elementary system: mass conservation in the gas channel (1D on the *y*-axis) and in the plane electrode (2D on the *x*- and *y*-axes) using the film model to represent the mass transfer between the gas channel and the electrode interface, the rates of chemical and electrochemical reactions, the Butler–Volmer model to describe the electrode kinetics and to estimate the current densities and electrical requirement for gas flow and electrochemical reactions.

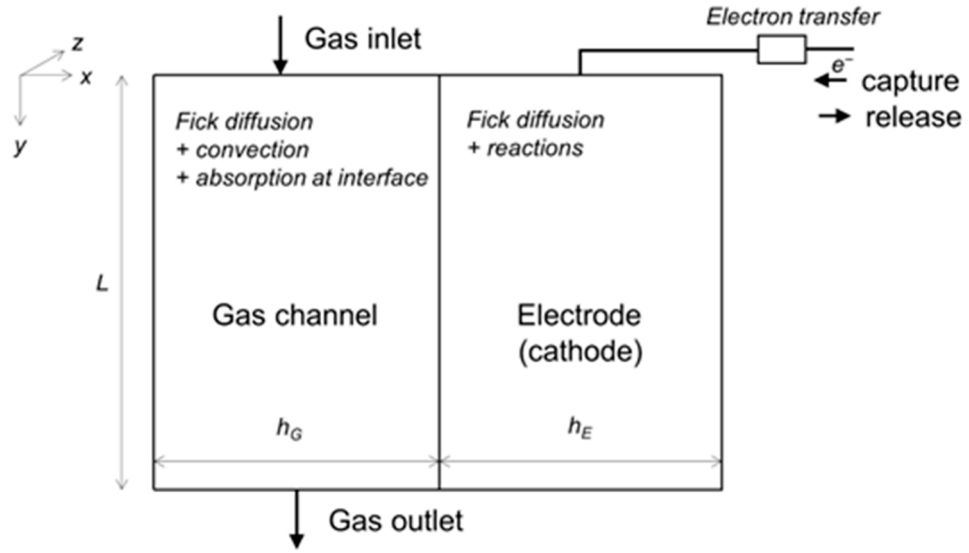

Figure 1. Schematic diagram of the rectangular cell geometry used for the modeling of electro-swing reactive adsorption, with L the channel length on the *y*-axis, h_G the gas channel thickness, h_E the electrode thickness on the *x*-axis, and l the channel width on the *z*-axis (electrolyte separator, anode, and current collector not shown).

During the capture phase, the gas with CO_2 is blown through a fan into the low-voltage cell, where the CO_2 first dissolves in the ionic liquid and then diffuses to selectively react with quinones immobilized on the electrode material. Once the material is saturated and CO_2 breakthrough occurs, the release phase begins. The gas flow is stopped, and the applied voltage is changed to facilitate CO_2 release from the electrode material. A non-reactive carrier gas, such as N_2, can be used with low sweep to facilitate CO_2 release without penetrating the ionic liquid.

2.1. Minimum Separation Work

For a substance to be separated from a mixture, e.g., CO_2 in a mixture of CO_2 and N_2, the theoretical minimum separation work to produce pure CO_2 as a function of the CO_2

capture rate between 0 and 100% can be calculated according to thermodynamic principles as follows [19]:

$$W_{min} = -\frac{RT}{3600My}\left(ln(x) + \frac{1-x}{x}ln(1-xy) + (1-y)ln\left(\frac{1-xy}{x(1-y)}\right)\right) \quad (1)$$

where W_{min} is the minimum separation work expressed per ton of pure CO_2 (in kWh/tCO_2), R is the gas constant (8.314 J/(mol·K)), T is the mixture temperature (K), x is the molar fraction of CO_2, M is the molecular weight of CO_2 (0.044 kg/mol), and y is the CO_2 capture rate.

Without considering overpotential and resistance losses in the cell, the theoretical minimum applied potential for the electrochemical reactions is obtained from the free enthalpy according to:

$$\Delta E_{min} = -\frac{\Delta G}{nF} = -\frac{3600M}{nF}W_{min} \quad (2)$$

where ΔE_{min} is the minimum applied potential (in V), ΔG is the free enthalpy (in J/molCO_2), F is Faraday's constant (96 485 C/mol), and n is the mole number of electron per CO_2 mole.

For a stoichiometry of one electron transferred per CO_2 molecule, the minimum separation work required at a CO_2 concentration of 420 ppmv in air and a temperature of 293.15 K varies between 124 kWh/tCO_2 for a 50% CO_2 capture rate and 134 kWh/tCO_2 for a 99% CO_2 capture rate. The corresponding minimum applied potentials are 0.20 V and 0.22 V, respectively. For higher concentrations of CO_2, typically around 1% in diluted flue gas, the minimum separation work is lower and varies between 76 kWh/tCO_2 for a 50% capture rate and 85 kWh/tCO_2 for a 99% capture rate. The corresponding minimum applied potentials are 0.12 V and 0.14 V, respectively. The minimum thermodynamic work represents a limit that is not reached under practical conditions, where differential cell voltages range from 1 to 2 V (i.e., 0.6 to 1.2 MWh/tCO_2) [10,11,20,21]. However, this highlights the importance of optimizing electrochemical techniques to further improve energy performance and reduce irreversible losses.

2.2. Assumptions

The main model assumptions and characteristics are discussed below:

1. The temperature and pressure applied to the cell are constant over time and homogeneous in space (isothermal and isobaric operation).
2. Only CO_2 can transport into the cell. Other gases present in the gas stream, such as N_2, O_2 and H_2O, are not considered. The ionic liquid is considered non-volatile and does not react chemically with the gases in the cell.
3. The average velocity in the gas stream is considered without regard to a radial velocity profile. With regard to axial dispersion and convection phenomena, the Bodenstein number (dimensionless ratio of dispersion to convection timescales) is an element of axial dispersion. Its value under the operating conditions evaluated (typically ~1 at low gas flow rate and greater than 1 at high gas flow rate) indicates that both phenomena must be considered.
4. The transfer of CO_2 from the gas channel to the electrode is described by means of the film model [22] and the liquid–vapor equilibrium of CO_2 at the gas channel–electrode interface is governed by Henry's law.
5. Electro-active CO_2 carrier molecules can undergo reversible two-electron transfers (radical anion formation in the first step and dianion formation in the second step). The potential at which these reductions occur and the corresponding kinetics of the electron transfer processes are dependent on the structure of the quinone and its interaction with the electrolyte. The reaction mechanism in the presence of CO_2

couples electrochemical and chemical reactions via the ECEC mechanism [10], where E is an electron transfer (reactions (3) and (5)) and C is a chemical reaction (reactions (4) and (6)). The ECEC mechanism, where the quinone captures two CO_2 molecules, involves the following substances: quinone (Q), one-electron reduced quinone ($Q^{\circ -}$), carboxylated quinone ($QCO_2^{\circ -}$), two-electron reduced quinone (QCO_2^{2-}), and quinone dianion diadduct ($Q(CO_2)_2{}^{2-}$). CO_2 addition is chemically reversible, as first reported by Mizen and Wrighton [7] and developed by Xu et al. [23]. Chemical reactions between quinones and CO_2 follow second-order kinetics. However, the reaction kinetics between CO_2 and electrogenerated nucleophiles is not completely known, especially the second addition, and the rate constants of the second chemical and electrochemical reactions are assumed to be equal to those of the first reaction.

$$Q + e^- \leftrightarrows Q^{\circ -} \text{ current } i_1, \text{ potential } E_1^\circ \tag{3}$$

$$Q^{\circ -} + CO_2 \leftrightarrows QCO_2^{\circ -} \text{ forward rate } k_1^f, \text{ reverse rate } k_1^r \tag{4}$$

$$QCO_2^{\circ -} + e^- \leftrightarrows QCO_2^{2-} \text{ current } i_2, \text{ potential } E_2^\circ \tag{5}$$

$$QCO_2^{2-} + CO_2 \leftrightarrows Q(CO_2)_2{}^{2-} \text{ forward rate } k_2^f, \text{ reverse rate } k_2^r \tag{6}$$

6. In the electrode, only diffusion in the ionic liquid controls the CO_2 flow, and the concentration of quinones in the electrode is considered homogeneous. With regard to diffusive mass transfer and chemical reaction phenomena, chemical reactions occur at a faster rate than the diffusion of CO_2 in the ionic liquid. This leads to a large Damköhler number (dimensionless ratio of diffusion to chemical reaction timescales), which is typically greater than 1 under the evaluated operating conditions. Therefore, the mass transfer of CO_2 into the electrodes is the rate-controlling step.
7. The switchable CO_2 binding is controlled by modulation of the electrode potential, which is considered as a globally homogeneous and constant value, while the current is calculated locally as a function of time. At the anode, the standard potential of the ferrocenium/ferrocene oxidizing/reducing couple is -0.03 V. Local electroneutrality is always maintained.
8. The current densities of electrochemical reactions are described by the Butler–Volmer equation [24]. This is a fundamental relationship between the current density (the amount of electric current passing through a cell per unit area of the electrode surface), the concentrations of the electroactive substances, and the overpotential (the difference between the electrode potential and the equilibrium potential). At low overpotentials, the reaction rate is limited by the activation energy barrier, whereas at high overpotentials, it can be diffusion-controlled.
9. The Faradaic efficiency of the system, defined as the moles of CO_2 captured per moles of electron transferred, is estimated at 90%.

To look at the two dimensionless numbers mentioned in the Assumptions, the Bodenstein number is calculated according to:

$$Bo = \frac{\tau_{dispersion}}{\tau_{convection}} = \frac{UL}{D_{aG}} \tag{7}$$

where $\tau_{dispersion}$ is the characteristic time of axial dispersion in gas phase (in s), $\tau_{convection}$ is the characteristic time of convection in gas phase (in s), U is the flow velocity in the channel (in m/s), L is the channel length (in m), and D_{aG} is the axial dispersion coefficient in gas phase (in m^2/s).

$Bo > 1$ implies efficient transport with limited mixing, whereas $Bo < 1$ implies dispersion and mixing.

The axial dispersion coefficient is calculated using the Aris–Taylor correlation adapted to parallel planes for laminar flow [25]:

$$D_{aG} = D_G + \frac{U^2 {h_G}^2}{210 D_G} \tag{8}$$

where D_G is the molecular diffusion coefficient of CO_2 in gas phase (in m^2/s) and h_G is the gas channel thickness (in m).

Typical parameter values are detailed in Tables 1 and 2. In addition, the Damkölher number is calculated according to:

$$Da = \frac{\tau_{diffusion}}{\tau_{reaction}} = \frac{{h_E}^2 k_1^f c_{Q^{\circ -}}}{D_{IL}} \tag{9}$$

where $\tau_{diffusion}$ is the characteristic time of CO_2 diffusion in the ionic liquid (in s), $\tau_{reaction}$ is the characteristic time of first carboxylation (in s), k_1^f is the bimolecular rate constant (in $m^3/(mol \cdot s)$), $c_{Q^{\circ -}}$ is the concentration of one-electron reduced quinone (in mol/m^3) assumed to be equal to the initial concentration of quinone, h_E is the electrode thickness (in m), and D_{IL} is the molecular diffusion coefficient of CO_2 in the ionic liquid (in m^2/s).

$Da > 1$ implies that the system is transport-limited, with the reaction occurring rapidly relative to the rate of transport of reactants, whereas $Da < 1$ implies that the system is reaction-limited, with the transport of reactants occurring more quickly.

2.3. Governing Equations of Capture and Release Phases

2.3.1. Mass Conservation

The mass balance is written for the CO_2 in the gas phase and in the electrode, as well as for the five immobilized species (quinone u, one-electron reduced quinone $u*$, carboxylated quinone v, two-electron reduced quinone $v*$, and quinone dianion diadduct w). In the channel gas stream, the CO_2 concentration (c_G) is described by the following equation, considering flow via Fick diffusion and convection, as well as mass transfer between the channel and the interface:

$$\frac{\partial c_G}{\partial t} = D_{aG}\left[\nabla^2 c_G\right]_y + U[\nabla c_G]_y - \frac{k_f}{h_G}\left(c_G - c_G^i\right) \tag{10}$$

where c_G is the CO_2 concentration in the gas phase (in mol/m^3), D_{aG} is the axial dispersion coefficient of CO_2 in the gas phase (in m^2/s), U is the flow velocity in the channel (in m/s), k_f is the mass transfer coefficient in the film (in m/s), h_G is the channel thickness (in m), and c_G^i is the CO_2 concentration at interface (in mol/m^3).

Inside the electrode, the CO_2 concentration (c_{IL}) is obtained from flow via Fick diffusion and reactions:

$$\frac{\partial c_{IL}}{\partial t} = D_{IL}\left[\nabla^2 c_{IL}\right]_{x,y} - k_1^f c_{u*} c_{IL} + k_1^r c_v - k_2^f c_{v*} c_{IL} + k_2^r c_w \tag{11}$$

where c_{IL} is the CO_2 concentration in the ionic liquid (in mol/m^3), D_{IL} is the diffusion coefficient of CO_2 in the ionic liquid (in m^2/s), k_1^f and k_2^f are the forward rate constants of chemical reaction (in $m^3/(s \cdot mol)$), and k_1^r and k_2^r are the reverse rate constants of chemical reaction (in s^{-1}).

In the electrode, the concentrations of the five immobilized species are as follows in the ECEC mechanism:

$$\frac{\partial c_u}{\partial t} = \frac{di_1}{FdV} \tag{12}$$

$$\frac{\partial c_{u*}}{\partial t} = -\frac{di_1}{FdV} - k_1^f c_{u*} c_{IL} + k_1^r c_v \tag{13}$$

$$\frac{\partial c_v}{\partial t} = \frac{di_2}{FdV} + k_1^f c_{u*} c_{IL} - k_1^r c_v \tag{14}$$

$$\frac{\partial c_{v*}}{\partial t} = -\frac{di_2}{FdV} - k_2^f c_{v*} c_{IL} + k_2^r c_w \tag{15}$$

$$\frac{\partial c_w}{\partial t} = k_2^f c_{v*} c_{IL} - k_2^r c_w \tag{16}$$

where c_u, c_{u*}, c_v, c_{v*}, and c_w are the concentrations of immobilized quinone, one-electron reduced quinone, carboxylated quinone, two-electron reduced quinone, and quinone dianion diadduct in the ionic liquid (in mol/m^3), i_1 and i_2 are the local currents (in A), and $dV = dxdyl$ is the local volume in the electrode (in m^3).

To assess reverse kinetic parameters from equilibrium constants and forward kinetic parameters, the quasi-steady-state approximation is employed:

$$K_1 = \frac{c_v}{c_{u*} c_{IL}} = \frac{k_1^f}{k_1^r} \tag{17}$$

$$K_2 = \frac{c_w}{c_{v*} c_{IL}} = \frac{k_2^f}{k_2^r} \tag{18}$$

where K_1 and K_2 are the equilibrium constants for the carboxylation of reactions (4) and (6) (in m^3/mol).

At the boundaries (inlet $y = 0$, outlet $y = L$, and gas–electrode interface i), the following equations are considered:

$$c_G|_{y=0} = c_{G0} \tag{19}$$

$$\left.\frac{\partial c_G}{\partial y}\right|_{y=L} = 0 \tag{20}$$

$$\left.\frac{\partial c_{IL}}{\partial y}\right|_{y=0, y=L} = 0 \tag{21}$$

$${C_{IL}}^i = \beta {C_G}^i \tag{22}$$

where c_{G0} is the inlet CO_2 concentration (in mol/m^3) and β is dimensionless Henry's constant of CO_2 in the ionic liquid.

2.3.2. Film Model: Mass Transfer and Thermodynamic Equilibrium at the Interface

The corresponding dimensionless group characterizing the film diffusion is the Sherwood number, *Sh*. The calculation of the Sherwood number and the mass transfer coefficient depends on the flow regime (turbulent or laminar), which is a function of the Reynolds number. If the Reynolds number becomes too small (at low flow rates), the mass transfer may not be sufficient to capture the CO_2 efficiently. For laminate structures, the following correlation can be used to estimate the mass transfer coefficient (k_f) in laminar flow at steady state [26]:

$$Sh = \frac{k_f d_h}{D_G} = 1.85\left(ReSc\frac{d_h}{L}\right)^{1/3} \tag{23}$$

where $Re = \rho_G U d_h / \mu_G$ is the Reynolds number ($Re < 1000$), $Sc = \mu_G/(D_G \rho_G)$ is the Schmidt number, d_h is the hydraulic diameter of gas channel (in m), and L is the channel length (in m).

The hydraulic diameter for a rectangular channel section is as follows:

$$d_h = \frac{2lh_G}{l + h_G} \tag{24}$$

where l is the channel width (in m) and h_G is the gas channel thickness (in m).

For calculating interface concentration between gas and liquid phases, the solubility of CO_2 in the ionic liquid follows Henry's Law in Equation (23) [27,28]. The solvent holds the dissolved CO_2 in equilibrium with the gas phase CO_2 partial pressure. Henry's Law used in an ideal infinitely dilute medium is as follows:

$$x^{mol}_{CO_2,IL} = \frac{P_{CO_2}}{H} \tag{25}$$

where $x^{mol}_{CO_2,IL}$ is the molar fraction of CO_2 in the ionic liquid, P_{CO_2} is the partial pressure of CO_2 in the gas (in bar), and H is Henry's constant (in bar).

β is derived from:

$$\beta = \frac{V^m_G P_G}{V^m_{IL} H} \tag{26}$$

where V^m_G is the ideal gas molar volume (in m^3/mol), V^m_{IL} is the ionic liquid molar volume (in m^3/mol), and P_G is the pressure in the gas channel (in bar).

2.3.3. Current Densities and Electrical Potentials

The local current densities due to electrochemical reactions in which an electron is exchanged can be written as follows according to the Butler–Volmer model [24]:

$$di_1 = FdAk^{\circ}_{u/u*} c^{\alpha_1}_{u*} c^{1-\alpha_1}_{u} \left[exp\left(\frac{(1-\alpha_1)F}{RT}\left(E - E^1_{eq}\right)\right) - exp\left(-\frac{\alpha_1 F}{RT}\left(E - E^1_{eq}\right)\right)\right] \tag{27}$$

$$di_2 = FdAk^{\circ}_{v/v*} c^{\alpha_2}_{v*} c^{1-\alpha_2}_{v} \left[exp\left(\frac{(1-\alpha_2)F}{RT}\left(E - E^2_{eq}\right)\right) - exp\left(-\frac{\alpha_2 F}{RT}\left(E - E^2_{eq}\right)\right)\right] \tag{28}$$

where $dA = ldy$ is a finite surface (in m^2), k° is the standard electrochemical rate (in m/s), α is the symmetry factor, T is the temperature (in K), and E is the electrical potential imposed to the cell (in V).

The redox potentials E^1_{eq} and E^2_{eq} are defined by the Nernst equation as the following:

$$E^1_{eq} = E^{\circ}_1 - \frac{RT}{F}\log\left(\frac{c_{u*}}{c_u}\right) \tag{29}$$

$$E^2_{eq} = E^{\circ}_2 - \frac{RT}{F}\log\left(\frac{c_{v*}}{c_v}\right) \tag{30}$$

where E°_1 and E°_2 are the standard reduction potentials (in V).

Mathematically, the Butler–Volmer equation (Equations (27) and (28)) is used to describe how the current density depends on the overpotential (difference between the applied potential and the redox potential). A higher overpotential can drive a faster reaction until limited by mass transport or reaction kinetics.

2.3.4. Electrical Requirement and Productivity

At the cell scale, the electrical requirement includes the power consumption over a cycle for electrochemical operation and gas flow through the cell using a fan. The pressure

drop in the channel gas stream can be evaluated by the following equation for laminar flow between two parallel plates [29]:

$$\Delta P = \frac{12\mu_G QL}{l{h_G}^3} \tag{31}$$

where ΔP is the pressure drop (in Pa), μ_G is the dynamic viscosity of gas (in Pa·s). Q is the gas flowrate (in m^3/s), and L, l, and h are the channel length, width, and thickness (in m).

Then, the electrical consumption caused by gas compression in an adiabatic system is as follows:

$$W_C = \frac{\gamma}{\gamma - 1} NRT \left(\left(\frac{P_{in}}{P_{out}} \right)^{1-\frac{1}{\gamma}} - 1 \right) \frac{1}{r} \tag{32}$$

where W_C is the electrical consumption (in J), γ is the adiabatic index of the gas, N is the number of moles passed through the channel (in mol), P_{in} and P_{out} are the pressure at inlet and outlet of the channel (in Pa), and r is the yield of the fan (estimated to 0.7).

The number of moles passed through the channel is derived from the following:

$$N = \frac{\rho_G Q \Delta t}{M_G} \tag{33}$$

where N is number of moles (in mol), ρ_G is the gas density (in kg/m^3), M_G is the gas molar weight (in kg/mol), and Δt is the phase duration (in s).

The fan is set up before the gas passes through the cell and the inlet pressure is calculated from the following:

$$P_{in} = P_{out} + \Delta P \tag{34}$$

where P_{out} is the atmospheric pressure (1 atm).

The electrical consumption over a cycle is the sum of the energy required for the electrochemical operation and to run the fan, evaluated as follows:

$$W_E = \sum_k U_k i_k \Delta t_k + W_C \tag{35}$$

where W_E is the electrical consumption (in J), U_k is the potential difference imposed on the cell (in V), i_k is the current at the finite time (in A), and Δt_k is the time step (in s).

The productivity, defined as the capture rate of a given unit volume of bed over the duration of a complete cycle, is calculated as the following:

$$\mathrm{Pr} = \frac{m_{CO_2}}{V_{bed} \Delta t} \tag{36}$$

where Pr is the productivity (in $kg/(m^3 \cdot day)$), m_{CO_2} is the mass of CO_2 produced during the release phase (in kg), V_{bed} is the volume of the bed (in m^3), and Δt is the complete cycle duration (in day).

2.4. Parameters

The capture and release of CO_2 depend on the redox potential of the quinone, the applied voltage (capture occurs when the quinone is reduced and can bind CO_2, and release occurs when the quinone is re-oxidized), the properties of the ionic liquid/electrode (quinone concentration, diffusion coefficient in the ionic liquid, Henry's constant of CO_2 in the ionic liquid, electrochemical kinetics, etc.), and the operating conditions (temperature, pressure). The physicochemical parameters used in the model are given in Table 1. Given the wide variety of quinones with an affinity for CO_2 and the partial level of knowledge about all their physicochemical properties, some of the model's input parameters are estimated in order of magnitude to represent the phenomena and capture the main effects

during the operation of the electrochemical cell (Table 1). Two cases are considered for the values of the equilibrium constant in the ECEC mechanism: weakly complexing quinones (i.e., the lowest value used as a reference in the simulation) and strongly complexing quinones (i.e., the highest value used for sensitivity). In addition, the cell parameters are given in Table 2. The thickness of the electrode (h_E in the x-axis) is kept at 150 µm, as in [10], to maintain the same time dependence of CO_2 diffusion in the ionic liquid. The thickness of the gas channel (h_G in the x-axis) strongly influences the pressure drop if it is too small. This parameter is set to 250 µm to limit the pressure drop. The width of the cell (l in the z-axis) is fixed at 0.1 m. This parameter affects both the pressure drop and the cell capacity. The length of the cell (L in the y-axis), which also affects both the pressure drop and electrode capacity, is fixed at 0.18 m.

Table 1. Physicochemical parameters used in the simulations.

Parameter		Value	Reference/Comment
c_{u0}	mol/m^3	100	[10]
D_G	m^2/s	1.6×10^{-5}	order of magnitude
D_{IL}	m^2/s	4×10^{-10}	[10,30]
E_1°	V	−1.21	[10]
E_2°	V	−1.21	[10]
H	Pa	3×10^6	[27,28]
K_1	m^3/mol	$10/10^{10}$	weakly complexing quinones/strongly complexing quinones [13]
k_1^f	m^3/(s·mol)	10^{-2}	anthraquinone compound [23]
K_2	m^3/mol	$10/10^{10}$	weakly complexing quinones/strongly complexing quinones [13]
k_2^f	m^3/(s·mol)	10^{-3}	assumed equal to k_1^f
$k_{u/u*}^\circ$	m/s	10^{-4}	[31]
$k_{v/v*}^\circ$	m/s	10^{-4}	assumed equal to $k_{u/u*}^\circ$
M_G	kg/mol	0.029	order of magnitude
P_{out}	atm	1	ambient conditions
T	K	298.15	ambient conditions
V_G^m	m^3/mol	2.45×10^{-2}	ideal gas
V_{IL}^m	m^3/mol	2.91×10^{-4}	[32]
α_1	-	0.5	[10]
α_2	-	0.5	[10]
γ	-	1.4	ideal diatomic gas
μ_G	Pa·s	1.9×10^{-5}	order of magnitude
ρ_G	kg/m^3	1.2	order of magnitude

Table 2. Cell parameters used in the simulations at the lab scale.

Parameter		Value
h_E	m	150×10^{-6}
h_G	m	250×10^{-6}
l	m	0.1
L	m	0.18
Q	m^3/s	10^{-8}–10^{-5}

2.5. Numerical Resolution and Verification

The method of lines is employed to solve the partial differential equations by discretizing all but one dimension. In this approach, the spatial domain is divided into finite volumes (with $N_x = N_y = 25$, chosen to ensure that further refinement does not

significantly alter the results), while the remaining temporal dimension is handled by a time-integration algorithm. Specifically, the resulting system of first-order ordinary differential equations is solved in MATLAB using the ode15s solver, which is well suited for stiff systems. During these simulations, the time step is adapted automatically to local gradients. Validation is carried out by verifying both mass and electric charge balances to ensure that the simulation correctly tracks both material (CO_2) and charge (electrons), confirming the solution's consistency and reliability. For the mass balance, the number of CO_2 moles remaining in the system at the end (including free CO_2 in the channel, free CO_2 dissolved in the electrode, and CO_2 bound to the quinones) must match:

- During the capture phase, the difference between the number of CO_2 moles injected at the channel inlet and the number of CO_2 moles leaving the channel at the outlet. This is dynamically tracked over time and then integrated over the entire stage.
- During the release phase, this corresponds to the number of CO_2 moles present in the cell at the beginning (accounting for the channel and electrode, including both free and bound CO_2) minus the number of CO_2 moles leaving the channel at the outlet. Again, this is dynamically tracked and integrated over time.

For the electric charge balance, the simulation ensures that the total charge associated with quinones being oxidized or reduced over the course of the process is equal to the net electrons injected into or recovered from the system, as determined by summing the current flow at each time step.

3. Results

Simulations are first carried out for CO_2 concentrations in the gas between 10 and 50%, in line with the numerical results presented by Voskian and Hatton [10] during the capture phase on breakthrough curves and current density profiles for a laboratory system. The simulation results obtained for a lower CO_2 concentration, typically 1%, are then presented and discussed.

3.1. Capture Breakthrough and Current Density Profiles from 10 to 50% CO_2

First, simulations are carried out under the operating conditions presented in the Voskian and Hatton study in a laminar flow system [10], at low gas flow rates (about 10^{-8} m^3/s) and inlet CO_2 concentrations between 10 and 50%, to estimate the breakthrough curve and current density profiles during the capture phase for a typical cell of 0.18 m × 0.10 m. The applied cell potential for CO_2 capture is negative, typically lower than −1.3 V [10], due to the non-spontaneous mechanism. The breakthrough curve corresponds to how the concentration of CO_2 changes over time at the outlet of the cell. The electrode is fully saturated when the outlet concentration normalized by the inlet concentration is 1. Data are plotted against the number of bed volumes processed, representing the ratio of the total volume of gas treated by the system to the gas channel volume.

Figure 2 (left) presents breakthrough curves of CO_2 concentration normalized by the inlet concentration as a function of bed volumes processed during the capture phase and shows the effect of the applied potential on the adsorption efficiency, with lower voltages improving CO_2 capture. Lower applied voltages (−1.3 V close to the results presented in [10]) lead to delayed breakthrough, indicating enhanced CO_2 capture. The time required to reach a normalized concentration of 0.95 is 1.2 h at −1.3 V compared to 1.4 h at −1.1 V. Furthermore, an applied potential of less than −1.3 V, which would increase the power consumption, does not alter the breakthrough curve. At 0 V, the breakthrough occurs earlier, indicating minimal CO_2 capture only due to the ionic liquid physical absorption (about 0.15 mmol compared to 0.54 mmol with electrochemistry). The dashed line represents no CO_2 capture without the ionic liquid, which serves as a reference consistent with a dispersed plug flow in the channel.

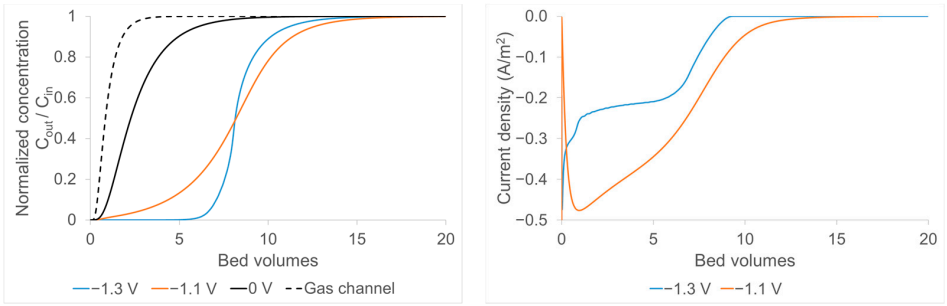

Figure 2. Capture breakthrough (**left**) and current density (**right**) profiles from simulation at 50% CO_2 and different charging potentials.

Figure 2 (right) shows the current density as a function of bed volumes during the capture phase under applied voltages of −1.3 and −1.1 V. The difference between the curves suggests a dependency of the current density profile on the applied voltage. Initially, both curves show a rapid variation in current density, reaching a peak around −0.5 A/m^2. The current density changes gradually with increasing bed volumes and approaches zero as the capture process stabilizes. As the electrode is filled with CO_2, the driving force for the reaction decreases, and the system approaches equilibrium. This reduces the electrochemical reaction rate and, consequently, the current density until it stabilizes at a level close to zero when no more CO_2 is captured.

Figure 3 (left top) shows breakthrough curves of normalized CO_2 concentration as a function of bed volumes for different CO_2 inlet concentrations in the feed gas: 50%, 20%, 15%, and 10%. The inlet concentration can influence the adsorption dynamics and the shape of the breakthrough curve. The breakthrough occurs later as the inlet concentration decreases, because of the fixed overall capacity. All breakthrough curves should theoretically collapse into a single curve when the bed volume is multiplied by the inlet concentration of CO_2 if transport and reactions are not limiting. This approach normalizes the capture process, accounting for the total amount of CO_2 adsorbed per unit volume of the cell across different inlet concentrations. However, the shift in the breakthrough curve suggests that transport and reaction limitations play a role (Figure 3 (top right)).

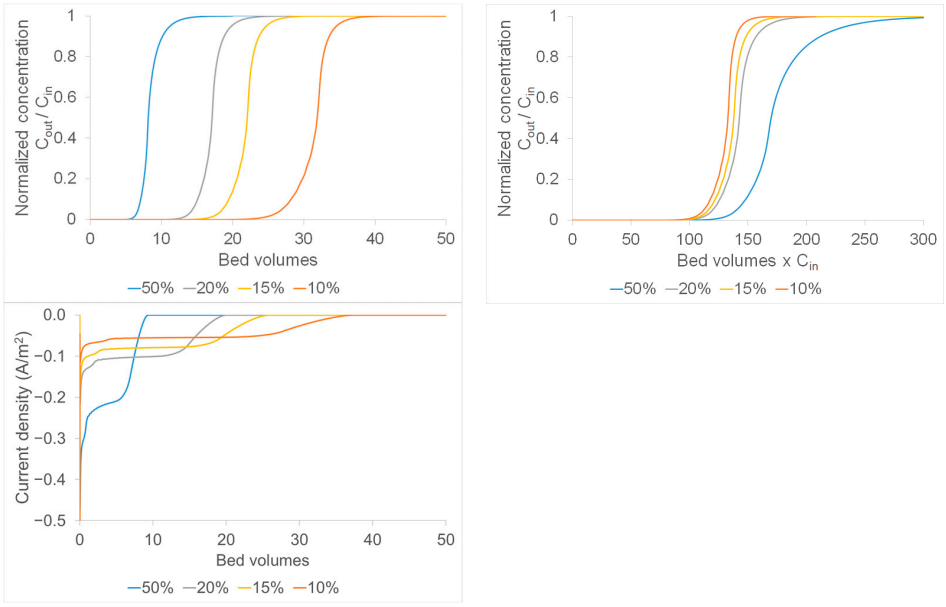

Figure 3. Capture breakthrough (**left top**), normalized breakthrough (**right top**), and current density (**left bottom**) profiles from simulation at different CO_2 inlet concentrations and at a charging potential of −1.3 V.

Figure 3 (left bottom) shows the current density as a function of bed volumes during the capture phase at different CO_2 inlet concentrations. It illustrates how the electrochemical response varies with different inlet concentrations of CO_2, showing that higher concentrations lead to higher initial peaks but reach saturation faster. Lower concentrations lead to a more prolonged, steady electrochemical response.

3.2. Capture and Release Phases at 1% CO_2

Simulations are then performed under operating conditions with a low inlet CO_2 concentration (1%) to evaluate the CO_2 and quinone concentration profiles and current density during capture and release. During capture, until full saturation, the flow rate in laminar flow is set at 10^{-7} m^3/s, and, during release, until full regeneration, a sweep gas is used at a flow rate of 1/100th of the capture flow rate. Indeed, a gas sweep is beneficial during the release phase, as it helps to desorb the gas by reducing its partial pressure, increasing the driving force and efficiently moving the desorbed molecules away from the surface. The sweep, which is easy to implement, can result in dilution and raises the question of the purity of the captured CO_2. Applying a rough vacuum to maintain low pressure in the channel and regenerate the adsorbent would also allow the partial pressure of CO_2 to be significantly reduced, thereby increasing capture efficiency and purity of CO_2 [33], but this method is not currently being investigated for the electro-swing reactive process compared to the gas sweep.

Figure 4 (left) shows the normalized CO_2 outlet concentration at an applied potential of −1.3 V as a function of the bed volumes treated (capture up to 500 bed volumes and release after 500 bed volumes). Initially, the outlet concentration is close to zero, indicating effective CO_2 capture. The concentration then gradually increases, indicating progressive saturation of the adsorption bed. At around 500 bed volumes, a sharp peak is observed, corresponding to the release phase, where CO_2 desorption occurs. At this operating point, a concentration effect (i.e., normalized concentration > 1) is observed at the beginning of the release phase.

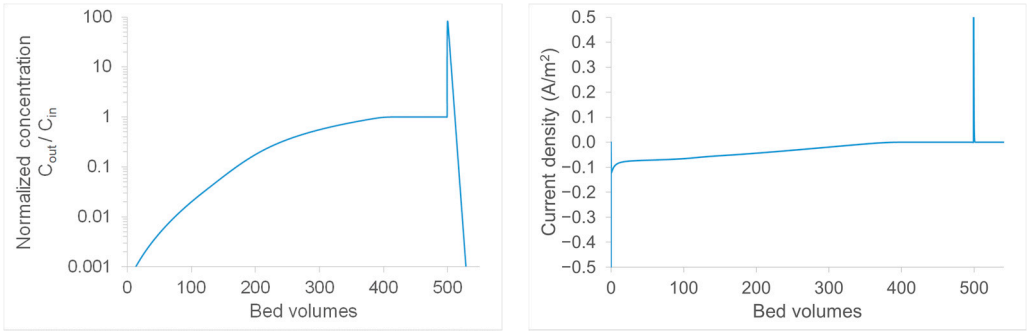

Figure 4. Normalized CO_2 concentration (**left**) and current density (**right**) profiles at a 1% CO_2 inlet concentration and at a charging potential of −1.3 V and a release potential of −0.5 V (ΔV of 0.8 V).

Figure 4 (right) shows the current density profile plotted as a function of bed volumes. During the initial capture phase, the current density remains negative and gradually increases as the electrode approaches saturation. At around 500 bed volumes, a sharp spike in the positive current density is observed, indicating the start of the release phase, where an electrical potential of −0.5 V is applied to drive the desorption of CO_2. For this operating point, the time required to reach a normalized concentration of 0.95 (about 0.52 mmol) is 4.7 h, and the productivity, including capture and release phases, is at 1.6 kg/(m^3·day) due to the long release phase duration that ensures a high working capacity (i.e., the productivity considering an instantaneous release phase reaches 9.7 kg/(m^3·day)). The

electrical consumption due to the electrochemical cycle is 0.6 MWh/tCO_2, and that due to fan is lower, at 0.05 MWh/tCO_2.

Figure 5 (left top) shows the normalized concentration profiles of the different quinone species involved in the electrode, plotted against the number of bed volumes (capture up to 500 bed volumes and release after 500 bed volumes). Initially, the concentration of quinone is high and then decreases rapidly over time as the capture process progresses. The one-electron reduced quinone is rapidly formed and then consumed. The two-electron reduced quinone shows a peak at intermediate bed volumes, indicating its formation and consumption. The quinone dianion shows increasing concentrations during the capture phase, reaching maximum values before the release phase. At about 500 bed volumes, a sharp decrease is observed for all the species, corresponding to the desorption phase, where the release of CO_2 is triggered. Figure 5 (right top) shows the normalized concentration at an applied potential of −1.1 V. The quinone species shows a gradual decrease but maintains a higher concentration throughout the capture phase compared to the −1.3 V case, indicating reduced reactivity at this less negative potential. The carboxylated quinone and the quinone dianion increase more gradually than in the previous case, indicating slower formation kinetics. The two-electron reduced quinone and the one-electron reduced quinone show lower and delayed peaks. This indicates that the system has a lower degree of quinone reduction and slower reactivity, leading to a more gradual transformation of the quinone species and affecting capture efficiency. The sharp concentration changes at around 500 bed volumes still represent the release phase. Moreover, in the ECEC mechanism, the equilibrium constants K_1 and K_2 of the quinone carboxylation reactions are important for the kinetics of the CO_2 release phase [7,13]. If the equilibrium constants are too high, the final CO_2 addition step is quasi-irreversible for the duration of the cycle. Thus, the rate constants of the reactions in the reverse direction can limit the efficiency of CO_2 release into the ionic liquid and slow down the release phase. Figure 5 (left bottom) shows the blockage of release for some strongly complexing quinones ($K \gg 1$) compared with weakly complexing quinones. Furthermore, an alternative ECE mechanism for the oxidation of quinone has been proposed to explain the regeneration of quinone and the release of CO_2 [7,10], but it has not yet been sufficiently investigated in terms of thermodynamics and kinetics (electrical potentials, electrochemical and chemical rates, enthalpies of reactions). Further understanding of the capture and, especially, the release mechanism is still important to improve model robustness.

To minimize the capture phase time, it would seem relevant to use a higher inlet flow, but this tendency comes into conflict with the pressure drop and residence time in the gas channel. Maintaining an efficient pressure drop is crucial when dealing with large volumes of gas to limit the electrical consumption of the fan. In fact, high pressure drops increase the power required to move the gas through the system, which can significantly increase operating costs. The accepted linear pressure drop is typically between 100 and 1500 Pa/m to ensure that the electrical consumption of the fans remains manageable [34,35]. To limit the linear pressure drop, the flow can be kept below 10^{-5} m^3/s (Figure 6, left top). The effect of increasing the gas flow rate on the efficiency of CO_2 capture is shown in Figure 6 (right top and left bottom), where the laminar gas flow rate (10^{-5} m^3/s) is increased by a factor of around 100 compared to the previous case.

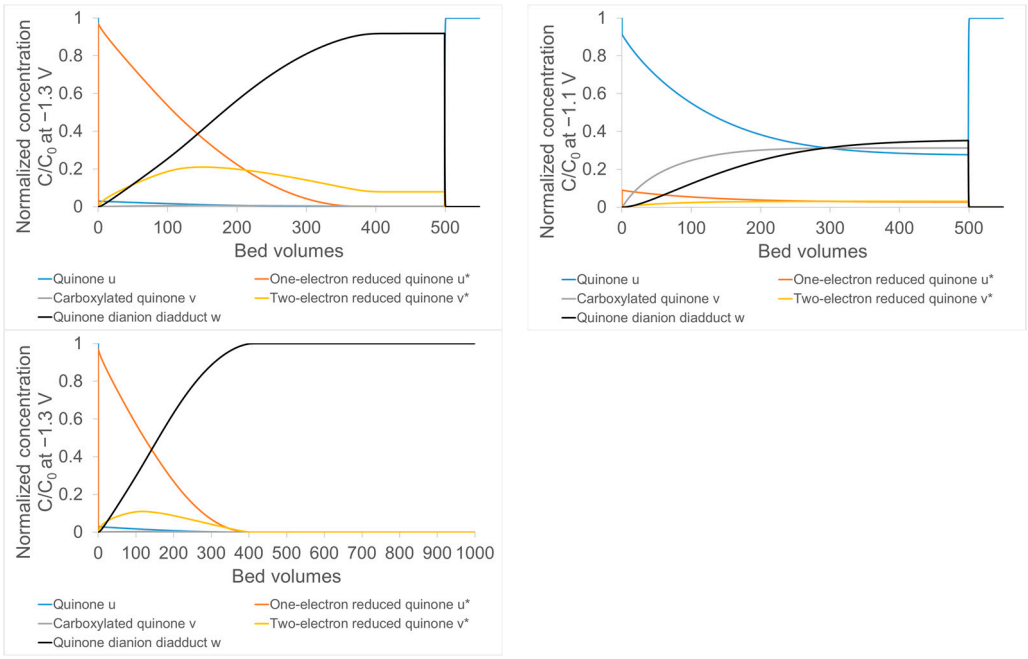

Figure 5. Quinone concentration profiles at a 1% CO_2 inlet concentration and at a charging potential of −1.3 V (**left top**, weakly complexing quinones) and −1.15 V (**right top**, weakly complexing quinones), and for a release potential of −0.5 V, using the equilibrium constant of strongly complexing quinones instead of weakly complexing quinones (**left bottom**, strongly complexing quinones).

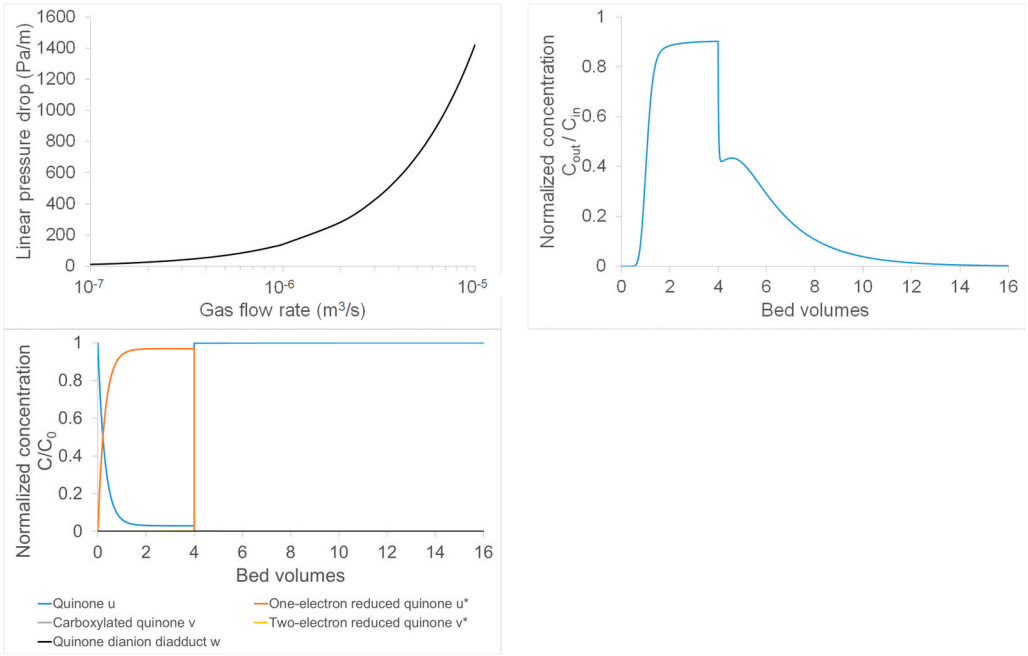

Figure 6. Linear pressure drop as a function of gas flow rate (**left top**), normalized CO_2 concentration (**right top**), and quinone concentration (**left bottom**) profiles at a 1% CO_2 inlet concentration, a charging potential of −1.3 V, a flow rate of 10^{-5} m^3/s, and a release potential of −0.5 V.

Figure 6 (right) shows typical breakthrough behavior. Initially, the outlet concentration is close to zero, indicating effective adsorption. After approximately two bed volumes, a rapid increase is observed, indicating breakthrough, where the material becomes saturated and the efficiency decreases. The curve then gradually declines after approximately four bed volumes, representing the release phase. However, the CO_2 released in the release phase is less concentrated in the sweep gas because the carboxylation of quinones is more

limited during the capture phase (Figure 6, right). This highlights the importance of the sweep gas flow rate during the release phase and underscores the potential interest in exploring alternatives such as partial vacuum regeneration. The reduced quinone formed electrochemically from the quinone reaches a plateau after about two bed volumes, but the carboxylated quinone formed with the CO_2 dissolved in the ionic liquid does not have time to form quantitatively, which limits the efficiency of capture, before the quinone is regenerated in the release phase. Indeed, the characteristic time of CO_2 diffusion in the ionic liquid is about 56 s, which is significantly longer than the residence time of CO_2 in the gas channel (about 0.5 s at a higher flow rate of 10^{-5} m^3/s) and the characteristic time of first carboxylation (about 1 s). Thus, further increases in the gas flow rate only amplify this mismatch between transport and reaction times, where the CO_2 molecules do not remain in contact with the wetted electrode long enough to diffuse and react effectively in the carboxylation reaction. This highlights the limitation imposed by the CO_2 diffusion coefficient within the wetted electrode ionic liquid and the importance of selecting the operating parameters for best performance. Consequently, CO_2 capture is low (about $4{\cdot}10^{-4}$ mmol) and the productivity including the capture and release phases is limited to 0.2 $kg/(m^3{\cdot}day)$ for this operating point. To address these challenges, new redox-active porous polymeric electrodes with interconnected pore sizes of 20–100 µm (i.e., favoring diffusion in the electrode) are being developed to enhance CO_2 transport, providing an increase in CO_2 transport and enabling productivity of up to 80 $kg/(m^3$-day) with a 0.2% CO_2 feed stream and an energy consumption of 1.3 MWh/tCO_2 (i.e., 4.8 GJ/tCO_2) [16].

4. Conclusions

This simulation-based study evaluates the performance of Faradaic electro-swing reactive adsorption for CO_2 capture under varying operating conditions. Results from a time-dependent model show that the applied potential, inlet CO_2 concentration, and gas flow rate significantly influence CO_2 capture efficiency.

Applying a negative potential of −1.3 V improves CO_2 capture, reducing the time to capture CO_2 by 15% compared to −1.1 V. Reducing the inlet CO_2 concentration from 50% to 10% delays the breakthrough times due to the fixed adsorption capacity of the system. However, normalizing the breakthrough curves by inlet concentration does not unify them, indicating the presence of transport and reaction limitations. At a low CO_2 concentration of 1%, effective capture is achieved with a productivity of 1.6 $kg/(m^3{\cdot}day)$ and an electrical energy consumption of 0.6 MWh/tCO_2.

Quinone species kinetics is critical; less negative potentials (e.g., −1.1 V vs. −1.3 V) reduce reactivity and capture efficiency, while strongly complexing quinones (i.e., those with high equilibrium constants) hinder CO_2 release during regeneration. Achieving a balance where electron transfer kinetics is fast enough to allow rapid capture, and complex formation thermodynamics are favorable for capture but not so strong as to inhibit CO_2 release, is crucial.

Furthermore, capture performance is mainly limited by mass transport, especially CO_2 diffusion in the ionic liquid and CO_2 dilution in the sweep gas. Increasing the gas flow rate beyond a certain threshold is counterproductive, resulting in high pressure drops and insufficient residence time, which negatively affect capture efficiency. This highlights the importance of balancing the flow rate, pressure drop, and residence time to optimize system performance within the gas channel and wetted electrode ionic liquid for a specific design. However, this analysis is limited by partial knowledge of the material properties and reactions involved in the ECEC mechanism. Future research should focus on overcoming CO_2 transport limitations, e.g., using quinone compounds with different complexation strengths and porous structures, and refining operational strategies to improve practical applicability.

Author Contributions: Conceptualization, O.A.; methodology, C.C. (Célisse Chevrel), P.d.J., C.C. (Christophe Castel) and O.A.; software, C.C. (Célisse Chevrel), P.d.J. and O.A.; validation, C.C. (Célisse Chevrel), P.d.J. and O.A.; formal analysis, C.C. (Célisse Chevrel), P.d.J., C.C. (Christophe Castel) and O.A.; investigation, C.C. (Célisse Chevrel); resources, O.A.; data curation, C.C. (Célisse Chevrel), P.d.J. and O.A.; writing—original draft preparation, C.C. (Célisse Chevrel) and O.A.; writing—review and editing, C.C. (Célisse Chevrel), P.d.J., C.C. (Christophe Castel) and O.A.; visualization, O.A.; supervision, P.d.J. and O.A.; project administration, O.A.; funding acquisition, O.A. All authors have read and agreed to the published version of the manuscript.

Funding: This research received no external funding.

Institutional Review Board Statement: Not applicable.

Informed Consent Statement: Not applicable.

Data Availability Statement: The original contributions presented in this study are included in the article. Further inquiries can be directed to the corresponding author.

Acknowledgments: The authors would like to thank François Lapicque of the Université de Lorraine, CNRS, LRGP for his help with the electrochemical processes.

Conflicts of Interest: The authors declare no conflicts of interest.

References

1. Kanniche, M.; Le Moullec, Y.; Authier, O.; Hagi, H.; Bontemps, D.; Neveux, T.; Louis-Louisy, M. Up-to-Date CO_2 Capture in Thermal Power Plants. *Energy Procedia* **2017**, *114*, 95–103. [CrossRef]
2. Renfrew, S.E.; Starr, D.E.; Strasser, P. Electrochemical Approaches toward CO_2 Capture and Concentration. *ACS Catal.* **2020**, *10*, 13058–13074. [CrossRef]
3. Zito, A.M.; Clarke, L.E.; Barlow, J.M.; Bím, D.; Zhang, Z.; Ripley, K.M.; Li, C.J.; Kummeth, A.; Leonard, M.E.; Alexandrova, A.N.; et al. Electrochemical Carbon Dioxide Capture and Concentration. *Chem. Rev.* **2023**, *123*, 8069–8098. [CrossRef] [PubMed]
4. Massen-Hane, M.; Diederichsen, K.M.; Hatton, T.A. Engineering Redox-Active Electrochemically Mediated Carbon Dioxide Capture Systems. *Nat. Chem. Eng.* **2024**, *1*, 35–44. [CrossRef]
5. Rosen, N.; Welter, A.; Schwankl, M.; Plumeré, N.; Staudt, J.; Burger, J. Assessment of the Potential of Electrochemical Steps in Direct Air Capture through Techno-Economic Analysis. *Energy Fuels* **2024**, *38*, 15469–15481. [CrossRef]
6. Saevarsdottir, G.; Magnusson, T.; Kvande, H. Reducing the Carbon Footprint: Primary Production of Aluminum and Silicon with Changing Energy Systems. *J. Sustain. Metall.* **2021**, *7*, 848–857. [CrossRef]
7. Mizen, M.B.; Wrighton, M.S. Reductive Addition of CO_2 to 9,10-Phenanthrenequinone. *J. Electrochem. Soc.* **1989**, *136*, 941–946. [CrossRef]
8. Scovazzo, P.; Poshusta, J.; DuBois, D.; Koval, C.; Noble, R. Electrochemical Separation and Concentration of <1% Carbon Dioxide from Nitrogen. *J. Electrochem. Soc.* **2003**, *150*, D91. [CrossRef]
9. Gurkan, B.; Simeon, F.; Hatton, T.A. Quinone Reduction in Ionic Liquids for Electrochemical CO_2 Separation. *ACS Sustain. Chem. Eng.* **2015**, *3*, 1394–1405. [CrossRef]
10. Voskian, S.; Hatton, T.A. Faradaic Electro-Swing Reactive Adsorption for CO_2 Capture. *Energy Environ. Sci.* **2019**, *12*, 3530–3547. [CrossRef]
11. Hemmatifar, A.; Kang, J.S.; Ozbek, N.; Tan, K.; Hatton, T.A. Electrochemically Mediated Direct CO_2 Capture by a Stackable Bipolar Cell. *ChemSusChem* **2022**, *15*, e202102533. [CrossRef] [PubMed]
12. Simeon, F.; Stern, M.C.; Diederichsen, K.M.; Liu, Y.; Herzog, H.J.; Hatton, T.A. Electrochemical and Molecular Assessment of Quinones as CO_2-Binding Redox Molecules for Carbon Capture. *J. Phys. Chem. C* **2022**, *126*, 1389–1399. [CrossRef]
13. Zito, A.M.; Bím, D.; Vargas, S.; Alexandrova, A.N.; Yang, J.Y. Computational and Experimental Design of Quinones for Electrochemical CO_2 Capture and Concentration. *ACS Sustain. Chem. Eng.* **2022**, *10*, 11387–11395. [CrossRef]
14. Abdinejad, M.; Seo, H.; Lev Massen-Hane, M.E.; Hatton, T.A. Oxygen-Stable Electrochemical CO_2 Capture Using Redox-Active Heterocyclic Benzodithiophene Quinone. *Angew. Chem. Int. Ed.* **2024**, *63*, e202412229. [CrossRef] [PubMed]
15. Jayarapu, K.N.; Mathur, A.; Li, X.; Liu, A.; Zhang, L.; Kim, J.; Kim, H.; Kuk, S.K.; Liu, Y. Indigo as a Low-Cost Redox-Active Sorbent for Electrochemically Mediated Carbon Capture. *Adv. Funct. Mater.* **2024**, *34*, 2402355. [CrossRef]
16. Guo, Y.; Massen-Hane, M.; Endy, G.; Hatton, T.A. Porous Polymeric Electrodes for Electrochemical Carbon Dioxide Capture. *Adv. Mater.* **2024**, *36*, 2407567. [CrossRef]

17. Jaworek, A.; Sobczyk, A.T.; Krupa, A.; Marchewicz, A.; Czech, T.; Śliwiński, L. Hybrid Electrostatic Filtration Systems for Fly Ash Particles Emission Control. A Review. *Sep. Purif. Technol.* **2019**, *213*, 283–302. [CrossRef]
18. Singh, S.; Stechel, E.B.; Buttry, D.A. Transient Modeling of Electrochemically Assisted CO_2 Capture and Release. *J. Electroanal. Chem.* **2017**, *799*, 156–166. [CrossRef]
19. Castel, C.; Favre, E. Membrane Separations and Energy Efficiency. *J. Membr. Sci.* **2018**, *548*, 345–357. [CrossRef]
20. Bui, A.T.; Hartley, N.A.; Thom, A.J.W.; Forse, A.C. Trade-Off between Redox Potential and the Strength of Electrochemical CO_2 Capture in Quinones. *J. Phys. Chem. C* **2022**, *126*, 14163–14172. [CrossRef] [PubMed]
21. Hartley, N.A.; Pugh, S.M.; Xu, Z.; Leong, D.C.Y.; Jaffe, A.; Forse, A.C. Quinone-Functionalised Carbons as New Materials for Electrochemical Carbon Dioxide Capture. *J. Mater. Chem. A* **2023**, *11*, 16221–16232. [CrossRef]
22. Whitman, W.G. The Two Film Theory of Gas Absorption. *Int. J. Heat Mass Transf.* **1962**, *5*, 429–433. [CrossRef]
23. Xu, Y.; Zheng, M.; Musgrave, C.B.; Zhang, L.; Goddard, W.A.; Bukowski, B.C.; Liu, Y. Assessing the Kinetics of Quinone–CO_2 Adduct Formation for Electrochemically Mediated Carbon Capture. *ACS Sustain. Chem. Eng.* **2023**, *11*, 11333–11341. [CrossRef]
24. Dickinson, E.J.F.; Wain, A.J. The Butler-Volmer Equation in Electrochemical Theory: Origins, Value, and Practical Application. *J. Electroanal. Chem.* **2020**, *872*, 114145. [CrossRef]
25. Brenner, H.; Edwards, D.A. *Macrotransport Processes*; Butterworth-Heinemann Series in Chemical Engineering; Butterworth-Heinemann: Boston, MA, USA, 1993; ISBN 978-0-7506-9332-5.
26. Coeuret, F.; Storck, A. *Éléments de Génie Électrochimique*; Génie des Procédés de l'École de Nancy; 2e Tirage Corr.; Tec et Doc: Paris, France, 1993; ISBN 978-2-85206-929-9.
27. Anthony, J.L.; Anderson, J.L.; Maginn, E.J.; Brennecke, J.F. Anion Effects on Gas Solubility in Ionic Liquids. *J. Phys. Chem. B* **2005**, *109*, 6366–6374. [CrossRef]
28. Lee, B.-C.; Outcalt, S.L. Solubilities of Gases in the Ionic Liquid 1-*n*-Butyl-3-Methylimidazolium Bis(Trifluoromethylsulfonyl)Imide. *J. Chem. Eng. Data* **2006**, *51*, 892–897. [CrossRef]
29. Bird, R.B.; Stewart, W.E.; Lightfoot, E.N. *Transport Phenomena*; Revised ed.; Wiley: New York, NY, USA, 2007; ISBN 978-0-470-11539-8.
30. Hou, Y.; Baltus, R.E. Experimental Measurement of the Solubility and Diffusivity of CO_2 in Room-Temperature Ionic Liquids Using a Transient Thin-Liquid-Film Method. *Ind. Eng. Chem. Res.* **2007**, *46*, 8166–8175. [CrossRef]
31. Wang, Y. *Advances in Electroanalytical Chemistry*; University of Oxford: Oxford, UK, 2012.
32. Jacquemin, J.; Husson, P.; Padua, A.A.H.; Majer, V. Density and Viscosity of Several Pure and Water-Saturated Ionic Liquids. *Green Chem* **2006**, *8*, 172–180. [CrossRef]
33. Deschamps, T.; Kanniche, M.; Grandjean, L.; Authier, O. Modeling of Vacuum Temperature Swing Adsorption for Direct Air Capture Using Aspen Adsorption. *Clean Technol.* **2022**, *4*, 258–275. [CrossRef]
34. Abdullatif, Y.; Sodiq, A.; Mir, N.; Bicer, Y.; Al-Ansari, T.; El-Naas, M.H.; Amhamed, A.I. Emerging Trends in Direct Air Capture of CO_2: A Review of Technology Options Targeting Net-Zero Emissions. *RSC Adv.* **2023**, *13*, 5687–5722. [CrossRef]
35. Wang, X.; Song, C. Carbon Capture From Flue Gas and the Atmosphere: A Perspective. *Front. Energy Res.* **2020**, *8*, 560849. [CrossRef]

Disclaimer/Publisher's Note: The statements, opinions and data contained in all publications are solely those of the individual author(s) and contributor(s) and not of MDPI and/or the editor(s). MDPI and/or the editor(s) disclaim responsibility for any injury to people or property resulting from any ideas, methods, instructions or products referred to in the content.